

R. Sundberg, S. Adler-Golden and P. Conforti, Long-wavelength infrared hyperspectral data "mining" at Cuprite, NV, Proc. SPIE 9611, Imaging Spectrometry XX, 961107 (1 September 2015).

Copyright 2015, Society of Photo-Optical Instrumentation Engineers. One print or electronic copy may be made for personal use only. Systematic reproduction and distribution, duplication of any material in this paper for a fee or for commercial purposes, or modification of the content of the paper are prohibited.

doi: 10.1117/12.2187061.

See next page.

Long-wavelength infrared hyperspectral data “mining” at Cuprite, NV

Robert Sundberg*, Steven Adler-Golden and Patrick Conforti
Spectral Sciences, Inc., 4 Fourth Avenue, Burlington, MA, USA 01803

ABSTRACT

In recent years long-wavelength infrared (LWIR) hyperspectral imagery has significantly improved in quality and become much more widely available, sparking interest in a variety of applications involving remote sensing of surface composition. This in turn has motivated the development and study of LWIR-focused algorithms for atmospheric retrieval, temperature-emissivity separation (TES) and material detection and identification. In this paper we evaluate some LWIR algorithms for atmospheric retrieval, TES, endmember-finding and rare material detection for their utility in characterizing mineral composition in SEBASS hyperspectral imagery taken near Cuprite, NV. Atmospheric correction results using the In-Scene Atmospheric Correction (ISAC) method are compared with those from the first-principles, MODTRAN[®]-based FLAASH-IR method. Covariance-whitened endmember-finding methods are observed to be sensitive to image artifacts. However, with clean data and all-natural terrain they can automatically locate and distinguish many minor mineral components, with especially high sensitivity to varieties of calcite. Not surprisingly, the major scene materials, including silicates, are best located using unwhitened techniques. Minerals that we identified in the data include calcite, quartz, alunite and (tentatively) kaolinite.

Keywords: Hyperspectral Imagery, Reflectance, Temperature-emissivity separation, Endmembers, Atmospheric Correction, Long-wavelength infrared, SEBASS, mineral identification

1. INTRODUCTION

Long-wavelength infrared (LWIR) hyperspectral imagery (HSI) has significantly improved in quality and become more widely available in recent years, and this in turn is sparking interest in a variety of applications involving remote sensing of surface composition. Among the best known and most extensive aircraft-based data sets are those acquired by Aerospace Corporation’s Spatially Enhanced Broadband Array Spectrograph System (SEBASS)¹, which covers both the midwave and longwave infrared (8-13 μm atmospheric window regions). In addition, a growing archive of imagery from the NASA Jet Propulsion Laboratory’s HyTES sensor [[www.http://airbornescience.jpl.nasa.gov/instruments/hytes](http://airbornescience.jpl.nasa.gov/instruments/hytes)], which covers the 8-11 μm region, has been assembled for public distribution. In addition, LWIR HSI data are now available from commercial sensors, such as the Telops HyperCam² and the Specim AisaOWL.³ However, the exploitation of LWIR HSI technology is still at an early stage, being much less developed than visible through short wavelength infrared (vis-SWIR) HSI, and questions remain about the overall utility of this wavelength region and the best choices of algorithms for data analysis.

One natural application for LWIR HSI is in mineral identification, since many minerals have specific chemical signatures in the LWIR. A handful of studies in this field have been conducted in recent years.^{3,4,5,6} Protocols developed for analyzing mineral scenes are relevant to the general problem of remotely detecting and identifying chemical compounds on the ground, such as for environmental monitoring and defense applications. Many of these applications call for fast, automated data processing, requiring no analyst supervision or expertise. Automatable steps include atmospheric retrieval and temperature-emissivity separation, location of “purest” materials (i.e., endmembers), both common and rare, material identification via comparisons to library spectra, and material abundance mapping.

In this paper we analyze SEBASS LWIR HSI data with automatable algorithms to identify minerals in the vicinity of Cuprite, Nevada, a location that has been well studied with both vis-SWIR HSI and ground surveys. Two different algorithms for atmospheric retrieval and temperature-emissivity separation (TES), FLAASH-IR⁷ and ISAC⁸, are compared. Algorithms for finding endmembers in whitened and unwhitened reflectance (i.e., 1 - emissivity) units, respectively, are used to locate purest instances of major and rare constituents and estimate their abundances. Rock and mineral identifications are made by comparing the endmembers with library spectra, and abundances are estimated by linear unmixing. Calcite, quartz, alunite and (tentatively) kaolinite have been located in the scene.

2. DATA ANALYSIS

Objectives

One objective of HSI analysis is classification, i.e., identification of the major material in each pixel. This may be done in several ways. One is to autonomously separate the pixels into spectrally distinct classes and then label the classes by comparing their average spectra with a library of known materials. Some type of biasing may be introduced to promote spatial contiguity of the classes. Another approach is to specify classes *a priori* via library spectra and then classify the pixels according via a goodness of fit criterion. In a variation on this method, the pixels may be linearly unmixed using library spectra, then classified according to the most abundant material. An advantage of this method is that the abundance maps can be more informative than the class assignments alone, as they indicate the extent of material mixing and the presence of minor materials, both of which are relevant to mineral scenes.

A different objective of HSI analysis is to find “rare” materials, which are materials that are outliers in the data and can be missed by standard classification methods. These materials are best found by applying a whitening transform to the data to suppress the common materials. The whitened data X' may be defined via

$$X' = ED^{-1/2}E^T(X-m) \quad (1)$$

where X is the original (radiance, emissivity or reflectance) data column vector, m is the image data mean, E is the matrix whose columns are eigenvectors of the data covariance, and D is the diagonal matrix of the corresponding covariance eigenvalues $\{d_1, d_2, \dots, d_n\}$, where powers of this matrix are defined as $D^Z = \text{diag}(d_1^Z, d_2^Z, \dots, d_n^Z)$. The E operation in Eq. (1) transforms the whitened data from eigenvector coordinates to the original wavelength coordinates. Whitened data are commonly used for rare target detection and anomaly finding. Anomalies are defined as pixels with large whitened amplitudes (Mahalanobis distances). These pixels can be further distinguished and identified using the same spectral endmember-finding, unmixing and matching algorithms that are applied to unwhitened data.

Dataset

The data we analyzed are SEBASS spectra acquired in the June, 2008 Joint Airborne Collection using Hyperspectral Systems (JACHS) experiment, which focused on mineral/lithologic identification and mapping along with environmental assessment in the western US.⁵ For this paper, two SEBASS LWIR data strips taken in the vicinity of Cuprite, NV, labeled 006_080614_130855_CPRT4m_05 and 006_080614_131925_CPRT4m_06, were analyzed independently of the Vis-SWIR or of any other imagery or ground measurements of the area. The LWIR images will be referred to as, respectively, “05” and “06.”

Atmospheric Retrieval and Temperature-Emissivity Separation

Identification of materials using remotely sensed hyperspectral data requires accounting for atmospheric effects so that comparisons can be made with spectra taken in the laboratory. The analysis makes use of the radiative transfer equation

$$L_{\text{obs}}(\lambda) = B(T, \lambda)\varepsilon(\lambda)\tau(\lambda) + [1 - \varepsilon(\lambda)]L^{\downarrow}(\lambda) + L^{\uparrow}(\lambda) \quad (2)$$

where λ is wavelength, $\varepsilon(\lambda)$ is the composition- and temperature-averaged spectral emissivity of the surface pixel, $\tau(\lambda)$ is the total (diffuse plus direct) transmittance between the surface and the sensor, $B(T, \lambda)$ is the surface Planck blackbody function at temperature T , $L^{\downarrow}(\lambda)$ is the transmitted incident (downwelling) illumination, and $L^{\uparrow}(\lambda)$ is the atmospheric path radiance. T is effectively an emissivity-weighted average within each pixel. Eq. (1) is rigorous for Lambertian surfaces; for specular surfaces the emissivity and illumination quantities may be regarded as “effective.” For a given atmosphere, characterized by the transmittance, path and illumination radiance spectra, Eq. (1) can be solved for a family of emissivity (or reflectance, $1-\varepsilon(\lambda)$) spectra corresponding to a range of possible surface temperature. Likewise, for a

given atmosphere and surface emissivity Eq. (1) defines a family of radiance spectra $L(\lambda)$ associated with that temperature range.

A number of algorithms for retrieving the atmospheric spectra and retrieving surface temperature have been developed, but none have been universally adopted. A simple and popular algorithm is the semi-empirical In Scene Atmospheric Correction (ISAC) method⁸, which has been used in most previous mineral mapping studies. ISAC uses approximate methods to find blackbody or near-blackbody pixels in the scene, and then performs linear regression with these pixels to estimate $\tau(\lambda)$ and $L^\uparrow(\lambda)$. The downwelling radiance is not retrieved and is neglected. For natural materials it is reasonable to perform the TES by setting either the maximum emissivity or the emissivity at a long wavelength, such as 12 μm , to a value close to 1; the former is the Normalized Emissivity Method, or NEM. Alternatively, TES may be avoided entirely by using a temperature-independent transformed spectrum, such as the alpha residual⁹, for material identification.

For low- to medium emissivity (i.e., reflective) materials, neglect of the downwelling radiance is a significant error, and a radiative transfer-based atmospheric retrieval method is needed. We use FLAASH-IR⁷, a first principles atmospheric retrieval and TES algorithm based on MODTRAN^{®10} developed for thermal IR HSI. FLAASH-IR uses a spectrally smooth emissivity constraint to retrieve a model atmosphere $\tau(\lambda)$, $L^\uparrow(\lambda)$ and $L^\downarrow(\lambda)$ from diverse pixels in the image. The same constraint is then used with the retrieved atmosphere to perform TES on the entire image.

The smooth-emissivity-based surface reflectance retrieval is sensitive to the magnitude of the downwelling signature appearing in the radiance spectrum. When the downwelling radiance is small and the surface spectra have prominent structure, as is often the case with desert or other dry scenes, the absolute reflectance determination is less precise. Here a TES method such as the NEM may be a better choice. In a recent study using FLAASH-IR, the NEM with the FLAASH-IR atmosphere gave better results than FLAASH-IR's baseline TES method.⁶ We observe similar behavior with the Cuprite data as well, and for our current analysis have adopted the NEM with maximum emissivity = 0.98. For the FLAASH-IR analysis the NEM is applied within the 8.1-13.0 μm range, which excludes the most atmospherically opaque wavelengths where the retrieval is not as well defined.

Figure 1 compares typical retrievals from image 06 using FLAASH-IR and the ISAC algorithm in ENVI (ENvironment for Visualizing Images, Exelis). Since the scene lacks either water or vegetation, it contains few if any true blackbody pixels, and this poses problems for ISAC's atmosphere retrieval. Indeed, both the atmospheric transmission and path radiance spectra from ISAC are unphysical at some wavelengths, where the former exceeds unity and the latter is negative (not shown). However, the ISAC reflectances, while lower than those from FLAASH-IR at the shorter wavelengths, do remain physically reasonable, and in many cases are a little smoother than FLAASH-IR's. We adopt the FLAASH-IR results for the remainder of this paper.

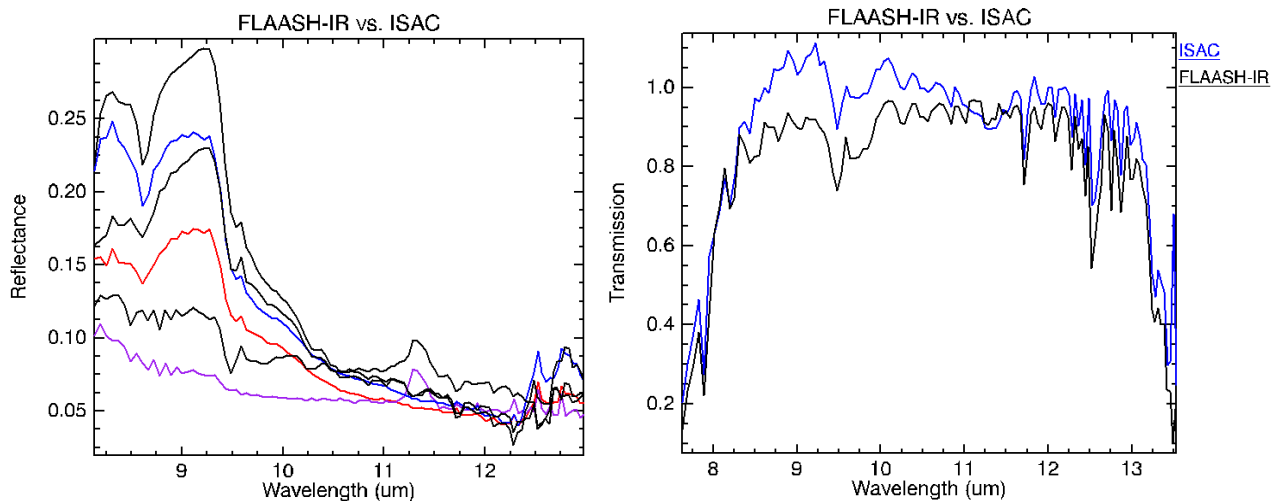


Figure 1. Comparison of typical ISAC and FLAASH-IR (black lines) retrievals from image 006_080614_131925_CPRT4m_06. At left, reflectances from FLAASH-IR (black) and ISAC (color) from the same three pixels. At right, retrieved atmospheric transmission

Objective (1): HSI Classification via Automated Endmember-Finding and Unmixing

As mentioned above, material classification in HSI may proceed by spectrally unmixing each pixel and then assigning a material from a library based on abundance.

We have used two algorithms in this study for this purpose. SMACC¹¹ is a fast, approximate convex cone method that derives endmembers and abundances with positivity and optional sum-to-unity or sum-below-unity constraints. Exact least-squares algorithms are considerably more time-consuming; however, an endmember method based on positivity-constrained binary unmixing (PCBU), which allows up to two endmembers abundances per pixel, is very efficient, and its strong sparseness constraint reduces the likelihood of a single material being misrepresented as a mixture. Our algorithm is similar to, but less optimized, than that described by Tits.¹²

The SMACC algorithm is described elsewhere.¹¹ At each endmember-finding step our PCBU algorithm, like SMACC, finds the pixel with the largest residual after unmixing, chooses that pixel as the latest endmember, and then recomputes the abundances and residuals before moving on to the next endmember. The key difference is that SMACC uses an approximate method of computation based on the previous abundances and residuals, while PCBU performs the calculations at each step from scratch using least squares, retaining only the best-fitting endmember combinations. With both algorithms the number of endmembers can be chosen to achieve a desired maximum residual size, and/or to provide a useful number of material types.

The SMACC algorithm in ENVI was applied to the reflectance images over the 8.1-13.0 μm range using the positivity constraint only. Figure 2 compares the first nine endmembers from each image. We have made material assignments for most of the 18 endmembers by comparisons with spectra from the Johns Hopkins University¹³ spectral libraries, as shown in Figure 3.

The first endmember in both images and the ninth from 06 are quartz. Three endmembers from 05 and one from 06 appear to be alunite. One endmember from 05 and two from 06 are calcite. In both images endmembers 2 are relatively smooth and flat. In image 06 this endmember is strongest on roads. While most concrete spectra have quartz-like features, a construction tar spectrum from the JHU library is also very flat. Endmember 4 from image 06 has two sharp peaks, at around 8.3 and 9.3 μm , very close to the quartz peak locations, but its shape somewhat resembles that of a library kaolinite spectrum. A different spectrum, which we found in image 05 by explicitly searching for kaolinite using the ENVI ACE (Adaptive Correlation Estimator) detector, provides a good match to kaolinite beyond 9 μm , as shown in Figure 3 at bottom right. Alunite, calcite and kaolinite have all been previously identified as abundant minerals at Cuprite based on vis-SWIR HSI.¹⁴ The endmember spectra from the PCBU algorithm were found to be similar to those from SMACC, although the order in which they are chosen can vary.

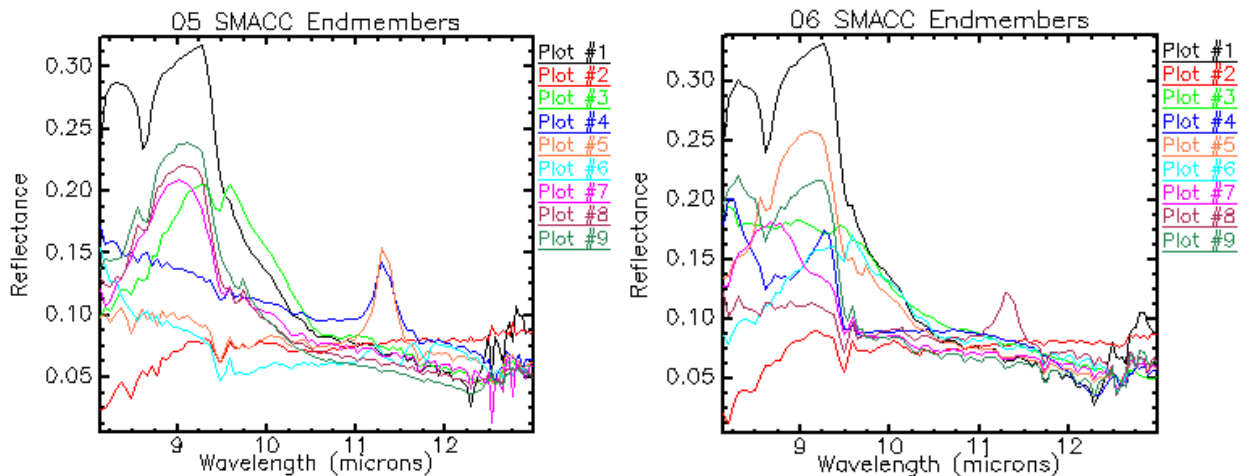


Figure 2. First nine SMACC reflectance endmembers from images 006_080614_130855_CPRT4m_05 (left) and 006_080614_131925_CPRT4m_06 (right).

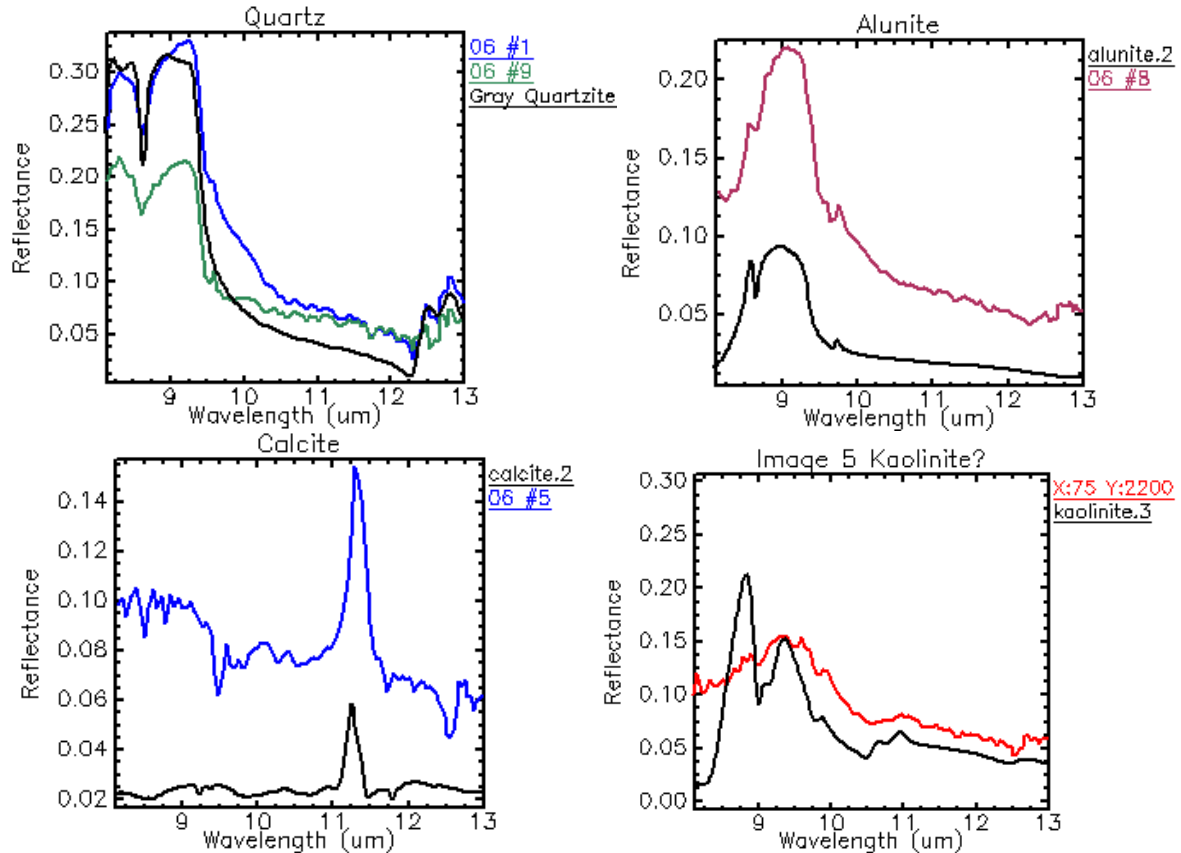


Figure 3. Comparisons of JHU library spectra (black curves) with reflectance data endmembers. The possible kaolinite spectrum was found with the ACE detector.

SMACC and PCBU-generated abundance maps of the calcite, alunite and primary (#1) quartz endmembers in image 06 are shown in RGB false color in Figure 4. The PCBU image was generated using the SMACC endmembers. It has an appearance intermediate between the SMACC abundance map and a typical classification map. Since the PCBU algorithm limits the abundances to two endmembers per pixel, there are many pixels that consist of only the other endmembers, and appear as black. The brighter areas of the SMACC abundance map correspond reasonably with the the PCBU abundances, although it appears that PCBU blends more calcite with the alunite and quartz at the expense of other endmembers. Both abundance maps are in qualitative agreement with results derived from VNIR-SWIR reflectance spectroscopy by Taranik.¹⁴

When too many endmembers are chosen (greater than around ten), some of the PCBU and SMACC abundance images take on a salt-and-pepper appearance, indicating that those endmember assignments are not well determined. This suggests that an optimum number of endmembers might be chosen based on spatial contiguity of the abundances.

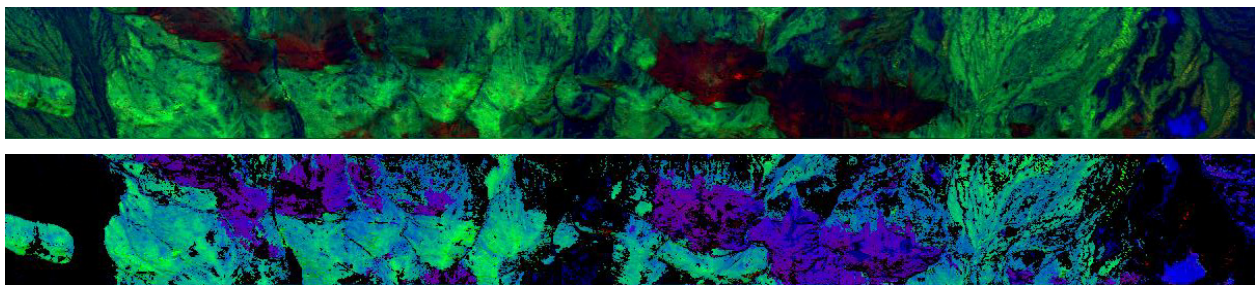


Figure 4. Abundances of quartz (red), alunite (green) and calcite (blue) endmembers from SMACC (top) and PCBU (bottom) in a portion of image 006_080614_131925_CPRT4m_06.

Objective (2): Rare Material Detection via Endmembers from Whitenes Data

As a separate objective, material detection can proceed from whitenes endmembers for HSI. Whitenes suppresses the major materials, such as quartz and alunite, and emphasizes sharp spectral features, such as those of calcite. The PCBU algorithm was run on the whitenes images to find endmembers and abundances, and the unwhitenes spectra of those endmembers were reported. Distinctive endmembers include examples of Endmember 4 from image 06, a triple-peaked spectrum not found previously, and a variant of calcite in which the typical 11.3 μm peak (see Figure 3) is inverted. The latter two spectra are shown in Figure 5 along with a calcite spectrum from the JHU library that has matching features in the 11.3 μm region. Since the major backgrounds are suppressed by whitenes, the abundance maps for all of the endmembers are very sparse.

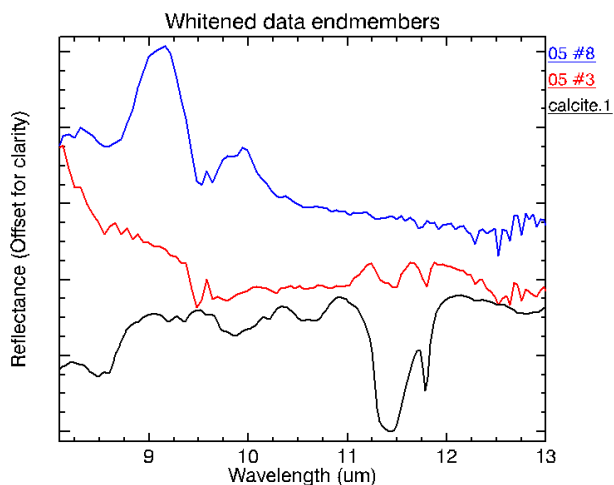


Figure 5. Selected endmembers from the whitenes reflectance image 006_080614_130855_CPRT4m_05. Curve in black is from the JHU library.

3. SUMMARY AND CONCLUSIONS

In this paper we used SEBASS data from Cuprite, NV to evaluate automatable algorithms for atmospheric retrieval, TES, endmember-finding and rare material detection for their utility in mineral characterization. Emissivity or reflectance retrievals using atmospheric spectra from the first-principles FLAASH-IR method differed from ISAC retrievals at the shorter wavelengths and should be more accurate. ISAC ignores the atmospheric downwelling radiance, and makes the assumption, which is questionable for this very dry environment, that blackbody pixels at different temperatures are present in the scene. Fast, automated endmember-finding and unmixing algorithms were shown to be of value in identifying "purest" materials, including both major and minor mineral components, the latter using whitenes data. Similar endmembers were found by the SMACC endmember and a binary unmixing-based algorithm. The latter generates sparse abundance maps that are intermediate between positivity-constrained abundance maps, from algorithms such as SMACC, and standard methods that assign a single class to each pixel. The end-to-end data analysis approach described in this paper is well suited to general applications in LWIR HSI that call for fast, automated data processing, with minimal or no analyst supervision or expertise.

4. ACKNOWLEDGMENT

The authors wish to acknowledge Spectral Sciences, Inc. for support under an internal research and development grant.

REFERENCES

- [1] Hackwell, J.A., D.W. Warren, R.P. Bongiovi, S.J. Hansel, T.L. Hayhurst, M.G. Sivjee, and J.W. Skinner, "LWIR/MWIR imaging hyperspectral sensor for airborne and ground-based remote sensing," Proc. SPIE, Imaging Spectrometry 2819, 102-107 (1996).
- [2] Chamberland, M., C. Belzile, V. Farley, J-F. Legault, K. Schwantes, Advancements in field-portable imaging radiometric spectrometer technology for chemical detection, Proc. SPIE 5416, 63, doi:10.1117/12.565033 (2004).
- [3] Holma, H., T. Hyvärinen, A-J. Mattila, O. Weatherbee, "Advances in hyperspectral LWIR pushbroom imagers," Proc. SPIE 8032, p. 80320X, doi:10.1117/12.884078 (2011).
- [4] Vaughan, R.G., W.M. Calvin, and J.V. Taranik, "SEBASS hyperspectral thermal infrared data: surface emissivity measurement and mineral mapping," Remote Sensing of Environment 85, 48-63 (2003).
- [5] Riley, D.N., O. Weatherbee, K.L. Jones, and W.A. Peppin, "Joint Airborne Collection using Hyperspectral Systems (JACHS): Geological and environmental mineral mapping with visible-shortwave infrared and a midwave-longwave infrared hyperspectral imagers," 33rd Int'l Geological Congress, Oslo (2008).
- [6] Cone, S.R., "Exploration of integrated visible to near-, shortwave-, and longwave-infrared (full range) spectral analysis," M.S. Thesis, Naval Postgraduate School, Monterey, CA (2014).
- [7] Adler-Golden, S., P. Conforti, M.-A. Gagnon, P. Tremblay and M. Chamberland, "Long-wave Infrared Surface Reflectance Spectra Retrieved from Telops Hyper-Cam Imagery," Proc. SPIE 9088, Algorithms and Technologies for Multispectral, Hyperspectral, and Ultraspectral Imagery XX, 90880U doi: 10.1117/12.2050446 (2014).
- [8] Young, S.J., B.R. Johnson and J. A. Hackwell, "An In-scene Method for Atmospheric Compensation of Thermal Hyperspectral Data," J. Geophys. Res. Atmospheres, 204, ACH 14-1 – ACH 14-20 (2002).
- [9] Hook, S. J., A.R. Gabell, A.A. Green, and P.S. Kealy, "A comparison of techniques for extracting emissivity information from thermal infrared data for geologic studies," Remote Sensing of Environment, 42, 123–135 (1992).
- [10] Berk, A., G.P. Anderson, P.K. Acharya, L.S. Bernstein, L. Muratov, J. Lee, M.J. Fox, S.M. Adler-Golden, J.H. Chetwynd, M.L. Hoke, R.B. Lockwood, T.W. Cooley and J.A. Gardner, "MODTRAN5: a Reformulated Atmospheric Band Model with Auxiliary Species and Practical Multiple Scattering Options," Proc. SPIE Int. Soc. Opt. Eng. 5655, 88 (2005).
- [11] Gruninger, J.H., A.J. Ratkowski, and M.L. Hoke, "The Sequential Maximum Angle Convex Cone (SMACC) Endmember Model," Proc. SPIE, Algorithms for Multispectral, Hyperspectral, and Ultraspectral Imagery 5425-1, Orlando FL, (2004).
- [12] Tits, L., R. Heylen, B. Somers, P. Scheunders, and P. Coppin, "A Geometric Unmixing Concept for the Selection of Optimal Binary Endmember Combinations," IEE Geosci. Remote Sens. Lett., 12, 82-86 (2015).
- [13] Johns Hopkins University spectral library, available from <http://speclib.jpl.nasa.gov> (2006).
- [14] Taranik, J.V., W.M. Calvin and F.A. Kruse, F.A., "Reflectance spectroscopy applied to exploration for mineral deposits and geothermal systems, and to the remediation of mined lands in the Great Basin of the United States," Proc. ASARS Symposium, Boulder, Colorado (Invited Paper) (2010).